Zitierweise: Angew. Chem. Int. Ed. 2023, e202309362
doi.org/10.1002/anie.202309362

VIP Non-Heme Iron Enzymes Very Important Paper

An $S=1$ Iron(IV) Intermediate Revealed in a Non-Heme Iron Enzyme-Catalyzed Oxidative C–S Bond Formation

Jared C. Paris[+], Sha Hu[+], Aiwen Wen[+], Andrew C. Weitz, Ronghai Cheng, Leland B. Gee, Yijie Tang, Hyomin Kim, Arturo Vegas, Wei-chen Chang, Sean J. Elliott,* Pinghua Liu,* and Yisong Guo**

Abstract: Ergothioneine (ESH) and ovothiol A (OSHA) are two natural thiol-histidine derivatives. ESH has been implicated as a longevity vitamin and OSHA inhibits the proliferation of hepatocarcinoma. The key biosynthetic step of ESH and OSHA in the aerobic pathways is the O_2-dependent C–S bond formation catalyzed by non-heme iron enzymes (e.g., OvoA in ovothiol biosynthesis), but due to the lack of identification of key reactive intermediate the mechanism of this novel reaction is unresolved. In this study, we report the identification and characterization of a kinetically competent $S=1$ iron(IV) intermediate supported by a four-histidine ligand environment (three from the protein residues and one from the substrate) in enabling C–S bond formation in OvoA from *Methyloversatilis thermotoleran*, which represents the first experimentally observed intermediate spin iron(IV) species in non-heme iron enzymes. Results reported in this study thus set the stage to further dissect the mechanism of enzymatic oxidative C–S bond formation in the OSHA biosynthesis pathway. They also afford new opportunities to study the structure-function relationship of high-valent iron intermediates supported by a histidine rich ligand environment.

Introduction

Ergothioneine (ESH, **5**, Scheme 1) and ovothiol A (OSHA, **8**, Scheme 1) are naturally-occurring thiol-histidine derivatives. Through an ESH-specific transporter OCTN1,[1] ESH accumulates in many tissues to concentrations as high as 100 μM—2 mM and exhibits protective roles in several aging associated diseases including dementia, depression, atherosclerosis, cardiovascular disorders, and nonalcoholic fatty liver disease.[2,3] Recently, Ames suggested that ESH might be a longevity vitamin.[4] OSHA is isolated from egg and ovaries of marine invertebrates and trypanosomatids.[5–7] It inhibits the proliferation of the human hepatocarcinoma cell line, Hep-G2, suggesting its antineoplastic potential.[8]

The biological activities of ESH and OSHA have sparked strong interest in their biosynthesis. In the last decade, two aerobic and two anaerobic ESH biosynthetic pathways, and one aerobic OSHA biosynthetic pathway have been reported (Scheme 1).[9–12] Among the aerobic pathways, the key chemical step lies in the formation of a unique carbon-sulfur bond (between cysteine and histidine for OSHA, or between γ-glutamyl-cysteine [γ-Glu-Cys] or cysteine and trimethylated histidine [TMH] for ESH) to produce the respective sulfoxide products (**3**, **4**, or **6**, Scheme 1). Mononuclear non-heme iron-containing enzymes have been identified to catalyze these transformations in an O_2-dependent manner: EgtB and Egt1 are used in ESH biosynthesis and OvoA is found in OSHA biosynthesis (Scheme 1). The crystal structures of EgtB from both *Mycobacterium thermoresistibile* ($EgtB_{Mth}$) and *Chloracidobacterium thermophilum* ($EgtB_{Cth}$) have been reported,[13,14] which revealed a mononuclear iron center coordinated by three His residues. Both substrates (TMH and γ-Glu-Cys for $EgtB_{Mth}$, or Cys for $EgtB_{Cth}$) bind to the iron center in a monodentate fashion (Figure S1), leaving one vacant coordination site for O_2 binding and activation. Based on sequence similarity and structural homology modeling,[15,16] OvoA has also been suggested to employ a 3-His binding motif for its iron center. Our recent spectroscopic studies suggested that both Cys and His, the two substrates for OvoA, bind to the

[*] J. C. Paris,[+] Dr. Y. Tang, Prof. Y. Guo
Department of Chemistry, Carnegie Mellon University
4400 Fifth Ave., Pittsburgh, PA 15213 (USA)
E-mail: ysguo@andrew.cmu.edu
Dr. S. Hu,[+] A. Wen,[+] Dr. A. C. Weitz, Dr. R. Cheng, H. Kim, Prof. A. Vegas, Prof. S. J. Elliott, Prof. P. Liu
Department of Chemistry, Boston University
590 Commonwealth Ave., Boston, MA 02215 (USA)
E-mail: elloitt@bu.edu
pinghua@bu.edu
Dr. L. B. Gee
LCLS, SLAC National Accelerator Laboratory
2575 Sand Hill Rd., Menlo Park, CA 94025 (USA)
Prof. W.-c. Chang
Department of Chemistry, North Carolina State University
Raleigh, NC 27695 (USA)
E-mail: wchang6@ncsu.edu
[+] These authors contributed equally to this work.

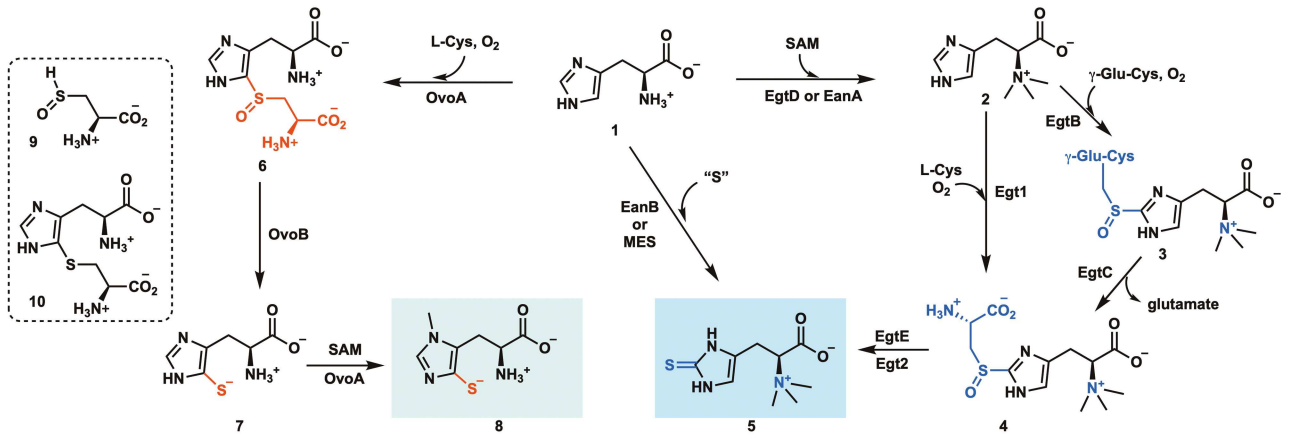

Scheme 1. The ESH and OSHA biosynthetic pathways. The proposed reaction intermediates in the OvoA catalyzed reaction are shown in the dashed box.

iron center as monodentate ligands.[16] This iron binding motif is distinct from the 2-His-1-carboxylate binding motif found in many well-characterized non-heme iron enzymes, such as iron- and 2-oxoglutarate-dependent (Fe/2OG) enzymes.[17,18] In Fe/2OG enzymes, it is well-established that the 2-His-1-carboxylate bound iron center enables O_2 activation via the oxidative decarboxylation of 2OG, which subsequently stabilizes a high-spin ($S=2$) oxoferryl (oxoiron(IV), or Fe(IV)=O) intermediate as the conserved reactive species to initiate the key chemical steps in enzyme catalysis.[19,20] However, the O_2 activation mechanism by a 3-His bound iron center and the resulting reactive intermediates are unknown. In recent years, the unique oxidative C–S coupling catalyzed by EgtB and OvoA has been examined using quantum mechanics/molecular mechanics (QM/MM)[21–23] and density functional theory (DFT)[24,25] calculations, where several reactive species, including Fe(IV)=O, Fe(III)-OOH, Fe(III)-$OO^{\bullet-}$, Fe(II)-OOH, and Fe(II)-$OO^{\bullet-}$, have been proposed as possible key intermediates. Thus far, none of them has been trapped and spectroscopically characterized, which significantly hampers critical mechanistic understanding of these reactions. Mechanistic information for 3-His or 4-His non-heme iron enzymes is also very limited.[26]

In this report, we characterized an OSHA biosynthetic mononuclear non-heme iron-containing enzyme from a mesophilic organism *Methyloversatilis thermotolerans* ($OvoA_{Mtht}$). Relative to the initially discovered OvoA from *Erwinia tasmaniensis* ($OvoA_{Eta}$),[27,28] $OvoA_{Mtht}$ has significantly improved thermostability[16] which facilitates its purification for mechanistic investigation. To elucidate the reaction pathway of $OvoA_{Mtht}$-catalysis, after kinetic characterization by stopped-flow absorption spectroscopy (SF-Abs), subsequent freeze-quench (FQ) coupled to Mössbauer and X-ray near-edge absorption spectroscopy (XANES) revealed the presence of an $S=1$ iron(IV) intermediate as the key intermediate to enable the oxidative C–S bond formation in OvoA. Based on the spectroscopic results, DFT calculations further suggest that this iron(IV) intermediate is most likely an oxoiron(IV) species. To our knowledge, this is the first $S=1$ iron(IV) intermediate reported for non-heme iron-containing enzymes.

Results and Discussion

Kinetic analysis reveals a novel intermediate (Int490) in $OvoA_{Mtht}$

$OvoA_{Mtht}$ was purified and concentrated to ≈1 mM.[16] The iron content of purified $OvoA_{Mtht}$ is ≈1.1 equivalent per $OvoA_{Mtht}$ subunit (see SI, Figure S2). Using the purified $OvoA_{Mtht}$, we first carried out pre-steady state enzyme kinetics studies using SF-Abs. The rapid mixing of the anaerobic $OvoA_{Mtht}$·Fe(II)·Cys·His quaternary complex with O_2 saturated buffer led to the formation of a transient optical species (termed Int490), exhibiting absorption features centered at ≈340 nm and 490 nm. Int490 reached a maximum accumulation at ≈0.02 s and decayed completely after 0.1 s (Figure 1a–b and Figure S6). Based on the relative amount of Int490 quantified from the Mössbauer analysis (see below), the estimated extinction coefficient of Int490 at 490 nm is ε_{490nm} ≈2000 $M^{-1}cm^{-1}$. Our prior EPR and Mössbauer characterization of $OvoA_{Mtht}$ suggested the presence of a direct Fe–S(Cys) ligation at the $OvoA_{Mtht}$ resting ferrous state,[16] we therefore suspect that these optical features are associated with charge transfer between iron and the ligated thiolate or thiolate derivatives (see below). A similar transient optical species (absorbing at 360 nm and 515 nm with ε_{515nm} ≈2700 $M^{-1}cm^{-1}$)[29] has been observed in the reaction catalyzed by isopenicillin *N* synthase (IPNS), which also contains a thiolate-ligated iron center from binding of the substrate, δ-(L-α-aminoadipoyl)-L-cysteinyl-D-valine. Mössbauer spectroscopy identified this IPNS transient optical species as a high-spin ($S=2$) oxoferryl intermediate.[29] Additionally, a different transient optical species with absorptions centered at ≈500 nm and ≈630 nm has been observed in IPNS, which was assigned to a ferric-superoxo intermediate.[29] In cysteine dioxygenase (CDO), another non-heme iron enzyme having a 3-His

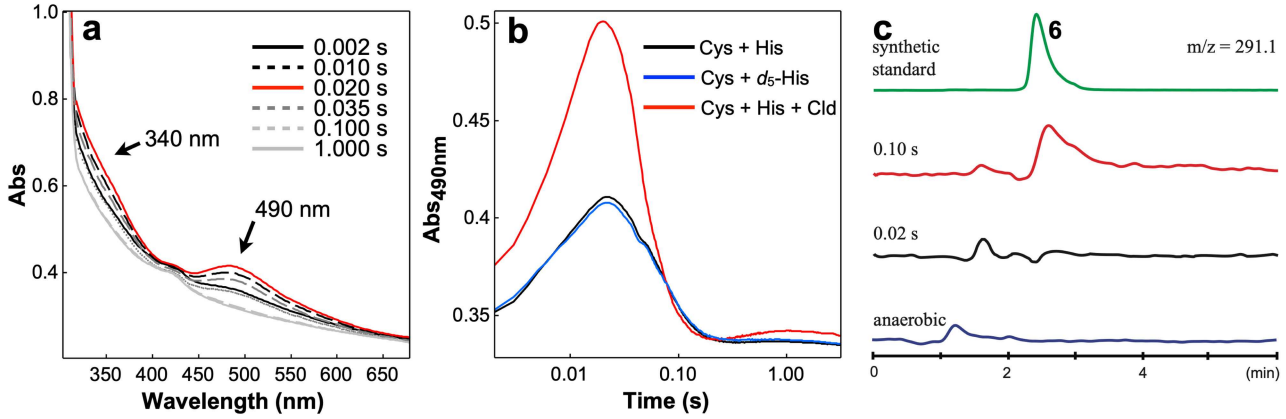

Figure 1. Kinetic and LC-MS analysis revealing a kinetic competent reactive intermediate in the $OvoA_{Mtht}$ reaction. (**a**) Stopped-flow absorption spectra of $OvoA_{Mtht}$ (0.3 mM) reacting with Cys (1.5 mM), His (9 mM), and O_2 (≈1.8 mM) at 4 °C. (**b**) Single wavelength A_{490} time trace (black) of $OvoA_{Mtht}$ reacting with Cys (1.5 mM), His (9 mM), and O_2 (≈1.8 mM) 4 °C. Chlorite dismutase (Cld) was added (10 μM) to the $OvoA_{Mtht}$·Cys·His ES complex and mixed with oxygen-saturated buffer containing chlorite (2 mM) to an excess oxygen solution (≈3 mM O_2). The corresponding single wavelength A_{490} time trace was shown as the red trace. The single wavelength A_{490} time trace of $OvoA_{Mtht}$ reacting with Cys (1.5 mM), [U-$^2H_5$]-His (9 mM), and O_2 (≈1.8 mM) is shown in blue. The kinetic simulations are shown in Figure S6. (**c**) LC-MS chromatograms of the $OvoA_{Mtht}$ catalyzed reactions in the presence of Cys and His quenched at 0.02 or 0.1 s. The MS detection was carried out using electrospray ionization (ESI^+).

bound iron center ligated by a Cys thiolate, a transient optical species with absorption features (500 nm and 640 nm) akin to those of the IPNS ferric-superoxo intermediate has also been reported.[30] While the nature of this optical species in CDO has not been determined experimentally, some models have been suggested based on computational studies, such as the iron-peroxythiolate species, Fe-OOSR (SI, Scheme S1).[30]

We also tested the deuterium kinetic isotope effect (D-KIE) on the decay kinetics of Int490. In many non-heme iron enzymes, if the key reactive intermediate, e.g. an oxoiron(IV) intermediate, is involved in a C–H activation step, the use of deuterium labeled substrate may lead to an increased accumulation (and the prolonged lifetime) of this intermediate due to D-KIE.[23,24] However, when [U-$^2H_5$]-His and Cys was used in the $OvoA_{Mtht}$ reaction, the decay kinetics of Int490 were not perturbed (Figures 1b and S6, see Sec. III.E in the Supporting Information for kinetics simulations). This observation is consistent with the near unity or inverse D-KIE in the $OvoA_{Eta}$ steady state studies,[15,33] suggesting that the oxidative C–S coupling is less likely to involve a C–H activation step at the substrate His. Overall, the nature of the $OvoA_{Mtht}$ Int490 cannot be readily determined by optical absorption features and the pre-steady state kinetics alone.

Mössbauer analysis of Int490

To elucidate the nature of Int490, we performed freeze-quench (FQ) coupled Mössbauer analysis. The anaerobic $OvoA_{Mtht}$·Fe(II)·Cys·His quaternary complex exhibited a quadrupole doublet with an isomer shift (δ) of 1.17 mm/s and quadruple splitting ($|\Delta E_Q|$) of 3.12 mm/s (Figures 2a and S7, and Table S1 in SI). These Mössbauer parameters represent a typical high-spin ($S=2$) ferrous species found in non-heme iron-containing enzymes and are also identical to the OvoA quaternary complex reported recently.[16] The rapid mixing of the complex with O_2-saturated buffer led to the formation of a new quadrupole doublet at 0.02 s (indicated by the red trace) with concomitant consumption of the quaternary complex (Figure 2a). The high energy absorption line of the new signal was well-resolved, but the low energy line overlapped with the ferrous signal from the quaternary complex. Using $\delta \approx 0.15$ mm/s and $|\Delta E_Q| \approx 1.35$–1.40 mm/s, a quadrupole doublet simulation reproduced this signal, which represented ≈25 % of the total iron in the sample (Table S1). This new quadrupole doublet decayed completely by 0.1 s, which matches the kinetic behavior of Int490 revealed in our SF-Abs studies (Figure 1). The decay of this species associated with Int490 led to the formation of another ferrous species having $\delta = 1.15$ mm/s and $|\Delta E_Q| = 2.18$ mm/s, which we assigned as an enzyme-product (EP) complex (Figure 2a, the blue doublet). This EP complex showed a relatively long lifetime, and slowly converted back to the quaternary complex in a time span of 10 s (Figure 2a). The Int490 formation is O_2-dependent, which is evidenced by the accumulation of Int490 to higher levels when chlorite dismutase (Cld) is used to generate higher O_2 concentrations in situ (Figure 1b).[34] Subsequent FQ-Mössbauer experiment using Cld to generate O_2 in situ allowed a maximal accumulation of Int490 to ≈60 % of the total iron in the sample at 0.02 s (Figures 2b and S8, and Table S2), which led to a more accurate determination of the Mössbauer parameters as $\delta = 0.16$ mm/s and $|\Delta E_Q| = 1.38$ mm/s. To our knowledge, transient species with similar parameters to those of Int490 have not been reported in non-heme iron enzymes. For comparison, the high-spin ($S=2$) oxoiron(IV) intermediates observed in Fe/2OG enzymes and related enzymes such as IPNS, exhibit isomer shifts in the range of

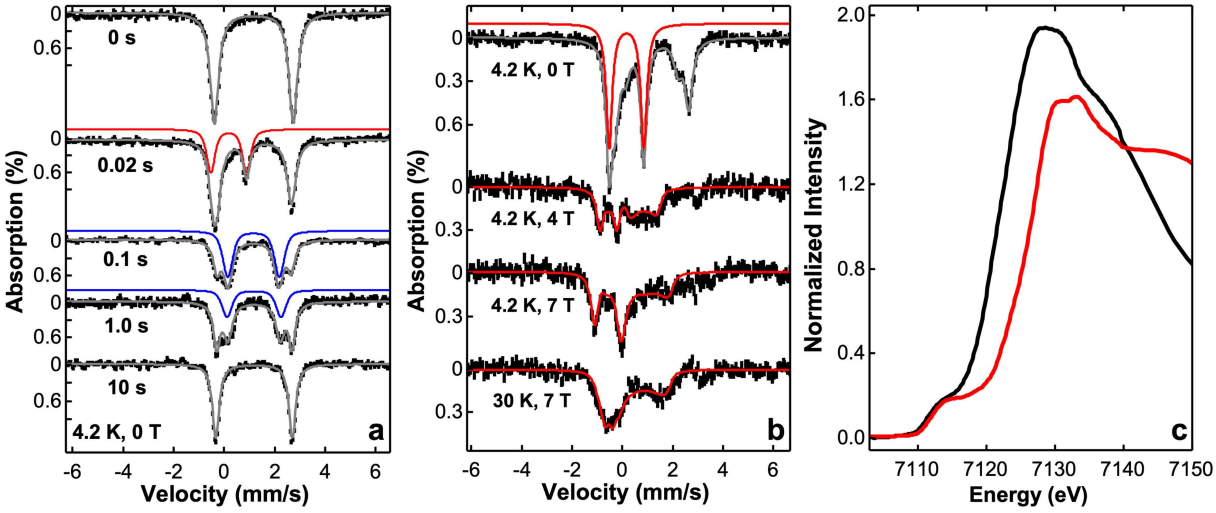

Figure 2. Mössbauer and XANES analysis of the reactive intermediate in the $OvoA_{Mtht}$ reaction. (**a**) 4.2 K zero field ^{57}Fe Mössbauer spectra of the reaction freeze quenched at various time points for the reaction of the $OvoA_{Mtht}$·Fe(II)·Cys·His complex reacting with O_2 saturated buffer. (**b**) Variable field and variable temperature ^{57}Fe Mössbauer spectra of the sample freeze quenched at 0.02 s for the reaction of the $OvoA_{Mtht}$·Fe(II)·Cys·His complex reacting with O_2 generated by Cld. The top spectrum is the raw spectrum of the sample measured at zero applied field while the bottom three spectra are the difference spectra showing only the spectral contribution of Int490. See Figure S9 for the procedure to generate these difference spectra. Within **a** and **b**, black = experimentally obtained data, grey = total spectral simulations, red = Int490 sub-spectra, blue = EP complex sub-spectra. (**c**) The normalized iron K-edge XANES spectra of the $OvoA_{Mtht}$·Fe(II)·Cys·His complex (black) and Int490 (red) after removing the contribution of the Fe(II) quaternary complex (See Sec. III.J. in the Supporting Information for more details on spectral analysis).

0.22–0.35 mm/s and quadrupole splittings in the range of 0.6–1.1 mm/s (Table 1).[19,35] Int490 is also incongruent with $S=2$ ferric-superoxo intermediates observed in IPNS and homoprotocatechuate 2,3-dioxygenase (HPCD), which exhibit isomer shifts of ≈0.5 mm/s.[29,36] In contrast, the Mössbauer parameters of Int490 are more akin to those of heme-based $S=1$ oxoferryl intermediates observed in myoglobin (Mb),[37] chloroperoxidases (CPOs),[38] horse radical peroxidase (HRP),[39] and bacterial cytochrome c peroxidases (bCCPs), such as MauG[40] and BthA,[41,42] as well as the 6-coordinate Fe(IV)-heme center with His and Tyr as the axial ligands (His/Tyr-Fe(IV)-heme) recently found in BthA.[42] In addition, the Mössbauer parameters of Int490 are also comparable to those of $S=1$ nonheme Fe(IV)=O synthetic model complexes supported by tetra-amine-cyclam ligands.[43,44]

Further details on the electronic structure of Int490 were derived from variable-temperature, variable-field (VTVH) Mössbauer measurements (Figures 2b and S9). By using an $S=1$ spin Hamiltonian, the spectral simulations satisfactorily reproduced the full set of VTVH Mössbauer data. The simulation parameters revealed that Int490 exhibited a large positive axial zero field splitting parameter ($D\approx 30\ cm^{-1}$), and an axial ^{57}Fe nuclear hyperfine tensor ($A_x/g_n\beta_n = A_y/g_n\beta_n = -26$ T, $A_z/g_n\beta_n = -5$ T). These parameters can be best compared with those determined for the heme-based $S=1$ oxoferryl intermediates from Mb,[37] HRP,[39] and BthA,[41,42] and His/Tyr-Fe(IV)-heme from BthA.[42] They are also similar to those from numerous reported $S=1$ nonheme Fe(IV)=O synthetic complexes (Tables 1 and S6).[35] To note, the use of an $S=2$ spin Hamiltonian yielded a parameter set with an unreasonably small ^{57}Fe nuclear

Table 1: Mössbauer and XANES parameters of Int490 and selected reactive species reported in the literature.

	Spin	δ (mm/s)	ΔE_Q (mm/s)	D (cm^{-1})	E/D	$A/g_n\beta_n$ (T)[a]	η	K pre-edge (eV)	K edge (eV)	Ref.
Int490[b]	1	0.16(1)	+1.38(3)	30(5)	0	−26(1), −26(1), −5(4)	0.5	7113.6(7)	7124(1)	This work
Mb Fe(IV)=O	1	0.09	+1.43	24	0	−19, −19, −3	0	7112	7124	[37]
HRP Fe(IV)=O	1	0.03	+1.61	22	0	−19, −19, −3	0	7113	7124	[39]
BthA Fe(IV)=O	1	0.07	+1.64	25	0	−23, −23, −6	0	–	–	[41,42]
TauD Fe(IV)=O	2	0.30	−0.90	10.5	0.01	−18.4, −17.6, −31	0	7114	7123	[48]
IPNS Fe(IV)=O	2	0.27	−0.44	10	0.09	−17.3, −12.9, −30.1	1.5	–	–	[29]
HPCD Fe(III)-$OO^{\bullet-}$	2	0.5	−0.33	−0.59	0.20	−21.4, −21.4, −21.4	−3	–	–	[36]
$[Fe(IV)(O)(TMC)]^{2+}$	1	0.17	+1.23	28	0	−25, −20, −3	0.5	7114	7124	[43]

[a] The Fermi contact term (A_{FC}) of the ^{57}Fe nuclear hyperfine tensor (**A**) of the ferryl intermediates can be estimated by taking the average of the three principal A values, assuming the pseudo contact (or orbital) term (A_{orb}) is small, thus negligible. Using this estimation, A_{FC} ranges from −13 to −20 T for the $S=1$ ferryl species and from −20 to −22 T for the $S=2$ ferryl species. [b] The numbers in parentheses are uncertainties in the least significant digit.

hyperfine tensor (Table S3). Specifically, the Fermi contact component of hyperfine tensor (A_{FC}) is only ≈ -7 T when using an $S=2$ spin Hamiltonian. As a comparison, for $S=2$ Fe(IV) species reported in the literature, such as $S=2$ enzymatic ferryl intermediates and related model complexes, A_{FC} is $\approx$ −20 - −25 T (Tables 1 and S6). This large discrepancy suggests that an $S=2$ spin state for Int490 is less likely (see Sec. III. J in the Supporting Information for more Mössbauer analysis).

EPR and XANES analysis of Int490

To further support the assignment that Int490 is at the Fe(IV) oxidation state, we employed cryogenic-radiolytic reduction (or cryoreduction) experiments to perform controlled one electron reduction of Int490.[45] After cryoreduction, ≈30 % of Int490 was converted to a high-spin ($S=5/2$) ferric species that was confirmed by both Mössbauer and electron paramagnetic resonance (EPR) characterizations (Figures S10–S14 and Tables S3–S5 in the SI). This observation suggests that the iron center in Int490 has a higher redox state than that of Fe(III), supporting its assignment as Fe(IV). As a third line of evidence, we have characterized a sample containing Int490 by XANES (due to the low concentration of Int490, ≈0.3 mM, useful EXAFS data cannot be obtained). Compared to the $OvoA_{Mtht}$·Fe(II)·Cys·His complex that shows an iron K-edge energy of 7122 eV (Figure 2c black trace), Int490 showed an iron K-edge energy of 7124 eV (Figure 2c red trace), which has a +2 eV shift relative to the Fe(II) state and is in the energy region of previously reported heme and non-heme ferryl intermediates (see also Figures S15–S16, Tables 1 and S7).[46] Additionally, the Fe K pre-edge area of Int490 (≈45 unit) is high, suggesting that a highly covalent Fe(IV)-ligand bond (such as Fe-oxo bond) may exist in Int490. As a comparison, the general range of the Fe K pre-edge area observed in many heme-based and non-heme ferryl species is ≈18–41 (Figure S15 and Table S7 in SI. Also see Sec. III. J. in the Supporting Information for more spectral analysis).[47]

LC-MS analysis on the OvoA reaction

The spectroscopic characterizations described above establish that Int490 is an $S=1$ Fe(IV) intermediate with spectroscopic parameters comparable to an $S=1$ oxoiron(IV) species. Next, we examined the kinetic competency of this Int490 intermediate in the production of sulfoxide **6**. After mixing the anaerobic OvoA·Fe(II)·Cys·His quaternary complex with O_2-saturated buffer, the reaction was quenched at selected time points (see the Supporting Information for the experimental details), and analyzed by liquid-chromatography coupled mass spectrometry (LC-MS, Figure 1c). At 0.02 s, when Int490 is maximally accumulated, final product **6** was below our detection limit. At 0.1 s, when Int490 had completely decayed, a compound with an elution time of ≈2.7 min and m/z value of 291.1 was identified. This peak has the same retention time and isotope distribution as the synthetic standard of **6** (see the Supporting Information for the biosynthesis and characterization of **6**, Figures S3–S5), confirming Int490 as a kinetically competent intermediate in OvoA-catalysis to produce sulfoxide **6**. In the last few years, several mechanisms for EgtB-catalysis have been proposed using QM/MM or DFT calculations[21,22,25] and similar models have also been suggested for OvoA.[12] Because the production of sulfoxide **6** in OvoA-catalysis is a four-electron oxidation process (sulfur oxidation and C–S coupling), these proposed EgtB and OvoA mechanistic models could be divided into two half reactions: either sulfur oxidation to sulfenic acid via O–O bond cleavage (**9**, Scheme 1) occurs prior to the formation of the C–S coupling (**10**, Scheme 1), or vice versa. We have chemically synthesized the thioether **10** by the reduction of compound **6** (see the Supporting Information for synthesis of **10**, Scheme S3, Figures S4–S5). If **10** is accumulated during the OvoA reaction, it provides support that the C–S coupling proceeds sulfur oxidation. However, under the experimental conditions examined, **10** was not detected in the chemical quench experiments due to either its high reactivity or due to its lack of involvement in the reaction (Figure S21). Therefore, we incline to favor that sulfur oxidation occurs prior to the C–S coupling in the OvoA catalysis. This order further implies that sulfur oxidation most likely happens in conjunction with the formation of the $S=1$ Fe(IV) intermediate as the result of O–O bond cleavage (see Scheme S2).

DFT analysis of Int490

Density functional theory (DFT) calculations (using both B3LYP and BP86 DFT functionals, see Sec. IV of the Supporting Information for details) were also performed to elucidate the nature of Int490. Based on our current observations that Int490 is an $S=1$ Fe(IV) intermediate and its decay leads to the formation of **6**, it strongly suggests that Int490 likely consists of a 6-coordinate iron center with four imidazole moieties from His (three from the OvoA protein backbone and one from the His substrate). The two remaining iron coordination sites could be occupied by either a sulfenic moiety derived from the Cys substrate and an oxo ligand (representing the result of O–O bond cleavage) to form an Fe(IV)=O species, or a peroxythiolate ($RSOO^-$) moiety in a bidentate fashion to form a cyclic Fe-OOSR species (Scheme S2). Based on these potential ligand environments, DFT calculations were carried out on several structural models (Figures S17–S20) by using the active site structure taken from the $EgtB_{Mth}$ crystal structure (see Sec. IV of the Supporting Information for details).[13] Regardless of the DFT functional used (B3LYP or BP86), the best models that satisfactorily reproduce the Mössbauer parameters of Int490 (δ, ΔE_Q, and the spin-dipolar component of the ^{57}Fe nuclear hyperfine tensor, Tables S8, S9) can be described as an $S=1$ Fe(IV)=O species (Figures S17, S19) together with a sulfenic moiety coordinated with the iron center via its oxygen (O=Fe(IV)-OSR, Model I by both B3LYP and BP86) or sulfur atom (O=Fe(IV)-S(O)R, Model II by BP86). The exception is the B3LYP result on

$S=1$ Model II (with the sulfenic moiety coordinating to iron via S), which can be best described as Fe(III)=O with an antiferromagnetically coupled sulfenic radical based on spin population analysis (O=Fe(III)-S(O•)R, Figure S19). Such a species is iso-electronic with the Fe(IV)=O species. A similar species (but with a different spin state) has been proposed in several computational studies as the key intermediate for the C–S coupling reaction.[22,23,25] However, the calculated Mössbauer parameters of this model are inconsistent with the experimental parameters of Int490 (Table S9). We also considered the structural models where a hydroxo ligand instead of an oxo ligand binds to the Fe(IV) center (Models V and VI, Figures S17, S19). However, the calculated Mössbauer parameters for the Fe(IV)-OH models are less consistent with the experimentally observed parameters for Int490 (Tables S8 and S9). More importantly, Fe(IV)-OH species generally exhibits small Fe K pre-edge areas (≈10 units),[47] thus inconsistent with the pre-edge area observed for Int490 (≈45 units). The calculations further demonstrated that the models (Models VII, and VIII by B3LYP functional, Figure S19) containing iron bound $RSOO^-$ all resulted in an $S=1$ Fe(II)-OOSR species with calculated Mössbauer parameters inconsistent with the experimental parameters from Int490 (Table S9). Finally, the calculated Mössbauer parameters from all the $S=2$ spin state models cannot reproduce the experimentally determined values (Tables S8–S9, Figures S18, S20). Therefore, for all the DFT calculations performed here, the best model which reproduced the Mössbauer parameters of Int490 is an $S=1$ oxoiron(IV) species supported by four His and one sulfenic moiety (Figure 3, also see Model I in Figures S17 and S19).

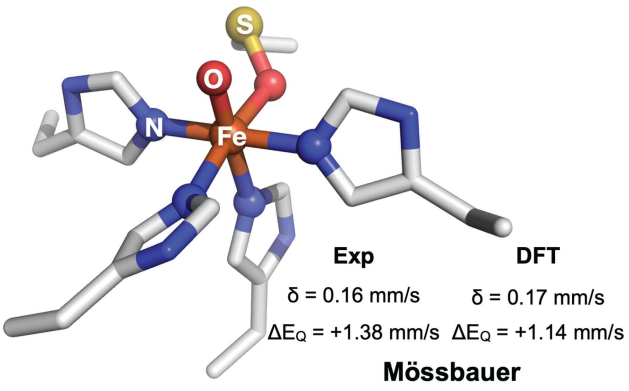

Figure 3. The best structural model of Int490 derived from DFT calculations and the comparison between the experimental and the DFT calculated Mössbauer parameters of Int490 (see Figures S17 and S19, and Tables S8 and S9).

Conclusion

In conclusion, the kinetic and spectroscopic studies revealed that an unprecedented $S=1$ Fe(IV) intermediate (Int490) most likely supported by a primary coordination environment of four histidines and a cysteine derived sulfenic acid is the key reactive species to enable the C–S coupling reaction catalyzed by OvoA. Such a reactive species is the first experimentally confirmed $S=1$ Fe(IV) intermediate in non-heme iron-containing enzymes and reflects the atypical reactivity of OvoA as a non-heme iron enzyme. In addition, the DFT studies further suggest that this high-valent iron intermediate is most likely an $S=1$ Fe(IV)=O species. A Fe(IV)=O intermediate (see Scheme S2) has been proposed in previous computational studies as the key reactive intermediate to carry out the C–S coupling reaction.[22,23,25] However, the involvement of an $S=1$ Fe(IV)=O species in such a reaction has never been proposed. Indeed, thus far, all other reported enzymatic non-heme Fe(IV)=O intermediates are in an $S=2$ spin state supported by a 2-His-1-carboxylate ligand set.[19,20] Relative to the carboxylic group of Asp or Glu, imidazole of His is a strong field ligand. Thus, a His-rich ligand environment (a total of four His in OvoA) could be the determining factor that leads to an $S=1$ Fe(IV) intermediate observed in this study instead of the more commonly observed $S=2$ spin state supported by the 2-His-1-carboxylic moiety. It is well established that $S=2$ ferryl intermediates are reactive and can perform radical chemistry, such as C–H bond activation. Although an $S=1$ enzymatic ferryl intermediate has not been identified prior to this study, similar biomimetic complexes in many cases exhibit weaker C–H activation reactivity than the $S=2$ counterparts.[49–51] Thus, it seems that nature has developed a radical-reactivity tamed ferryl intermediate ($S=1$) to perform other non-radical oxidative transformations, such as the C–S coupling reaction found in OvoA. Taken together, the identification of an $S=1$ Fe(IV) intermediate set the stage to further dissect the mechanism of enzymatic oxidative C–S bond formation by OvoA and related enzymes. It also expands our understanding on the non-heme high-valent iron intermediates supported by a ligand environment beyond 2-His-1-carboxylate ligand set.

Acknowledgements

This work is supported by National Science Foundation grants: CHE-1654060 (Y.G.) and CHE-2004109 (P.L.); National Institutes of Health grants: R35GM136294 (S.J.E), R01GM140040 (P.L.), and R01GM127588 (W.-c.C.). This work used Bridges-2 at Pittsburgh Supercomputing Center through allocation [CHE-200003] from the Advanced Cyberinfrastructure Coordination Ecosystem: Services & Support (ACCESS) program, which is supported by National Science Foundation grants #2138259, #2138286, #2138307, #2137603, and #2138296. We thank Dr. Ryan Ribson from SLAC National Accelerator Laboratory for the assistance in the XANES measurements. Use of the Stanford Synchrotron Radiation Lightsource, SLAC National Accelerator

Laboratory, is supported by the U.S. Department of Energy, Office of Science, Office of Basic Energy Sciences under Contract No. DE-AC02-76SF00515. We also thank Zachary Van Horn from the Penn State Radiation Science and Engineering Center for the assistance in the cryogenic-radiolytic reduction experiments.

Conflict of Interest

The authors declare no conflict of interest.

Data Availability Statement

The data that support the findings of this study are available in the supplementary material of this article.

Keywords: Ergothioneine · Ferryl Intermediates · High-Valent Iron · Ovothiol A · Oxidative C–S Bond Formation

[1] D. Gründemann, S. Harlfinger, S. Golz, A. Geerts, A. Lazar, R. Berkels, N. Jung, A. Rubbert, E. Schomig, *Proc. Natl. Acad. Sci. USA* **2005**, *102*, 5256–5261.
[2] I. K. Cheah, B. Halliwell, *Biochim. Biophys. Acta Mol. Basis Dis.* **2012**, *1822*, 784–793.
[3] I. K. Cheah, B. Halliwell, *Antioxidants* **2020**, *9*, 595.
[4] B. N. Ames, *Proc. Natl. Acad. Sci. USA* **2018**, *115*, 10836–10844.
[5] H. S. C. Spies, D. J. Steenkamp, *Eur. J. Biochem.* **1994**, *224*, 203–213.
[6] D. J. Steenkamp, H. S. C. Spies, *Eur. J. Biochem.* **1994**, *223*, 43–50.
[7] J. V. Goldstone, A. Hamdoun, B. J. Cole, M. Howard-Ashby, D. W. Nebert, M. Scally, M. Dean, D. Epel, M. E. Hahn, J. J. Stegeman, *Dev. Biol.* **2006**, *300*, 366-384.
[8] G. L. Russo, M. Russo, I. Castellano, A. Napolitano, A. Palumbo, *Mar. Drugs* **2014**, *12*, 4069–4085.
[9] R. Burn, L. Misson, M. Meury, F. P. Seebeck, *Angew. Chem. Int. Ed.* **2017**, *56*, 12508–12511.
[10] R. Cheng, L. Wu, R. Lai, C. Peng, N. Naowarojna, W. Hu, X. Li, S. A. Whelan, N. Lee, J. Lopez, C. Zhao, Y. Yong, J. Xue, X. Jiang, M. W. Grinstaff, Z. Deng, J. Chen, Q. Cui, J. Zhou, P. Liu, *ACS Catal.* **2020**, *10*, 8981–8994.
[11] M. A. Beliaeva, F. P. Seebeck, *JACS Au* **2022**, *2*, 2098–2107.
[12] N. Naowarojna, R. Cheng, L. Chen, M. Quill, M. Xu, C. Zhao, P. Liu, *Biochemistry* **2018**, *57*, 3309–3325.
[13] K. V. Goncharenko, A. Vit, W. Blankenfeldt, F. P. Seebeck, *Angew. Chem. Int. Ed.* **2015**, *54*, 2821–2824.
[14] A. R. Stampfli, K. V. Goncharenko, M. Meury, B. N. Dubey, T. Schirmer, F. P. Seebeck, *J. Am. Chem. Soc.* **2019**, *141*, 5275–5285.
[15] L. Chen, N. Naowarojna, H. Song, S. Wang, J. Wang, Z. Deng, C. Zhao, P. Liu, *J. Am. Chem. Soc.* **2018**, *140*, 4604–4612.
[16] R. Cheng, A. C. Weitz, J. Paris, Y. Tang, J. Zhang, H. Song, N. Naowarojna, K. Li, L. Qiao, J. Lopez, M. W. Grinstaff, L. Zhang, Y. Guo, S. Elliott, P. Liu, *Chem. Sci.* **2022**, *13*, 3589–3598.
[17] S. Gao, N. Naowarojna, R. Cheng, X. Liu, P. Liu, *Nat. Prod. Rep.* **2018**, *35*, 792–837.
[18] C. Q. Herr, R. P. Hausinger, *Trends Biochem. Sci.* **2018**, *43*, 517–532.
[19] C. Krebs, D. Galonić Fujimori, C. T. Walsh, J. M. Bollinger, *Acc. Chem. Res.* **2007**, *40*, 484–492.
[20] S. Kal, L. Que, *J. Biol. Inorg. Chem.* **2017**, *22*, 339–365.
[21] A. S. Faponle, F. P. Seebeck, S. P. De Visser, *J. Am. Chem. Soc.* **2017**, *139*, 9259–9270.
[22] G. Tian, Y. Liu, *ACS Catal.* **2018**, *8*, 5875–5889.
[23] P. Wu, Y. Gu, L. Liao, Y. Wu, J. Jin, Z. Wang, J. Zhou, S. Shaik, B. Wang, *Angew. Chem. Int. Ed.* **2022**, *61*, e202214235.
[24] E. A. C. Bushnell, G. B. Fortowsky, J. W. Gauld, *Inorg. Chem.* **2012**, *51*, 13351–13356.
[25] W. J. Wei, P. E. Siegbahn, R. Z. Liao, *Inorg. Chem.* **2017**, *56*, 3589–3599.
[26] D. Buongiorno, G. D. Straganz, *Coord. Chem. Rev.* **2013**, *257*, 541–563.
[27] A. Braunshausen, F. P. Seebeck, *J. Am. Chem. Soc.* **2011**, *133*, 1757–1759.
[28] N. Naowarojna, P. Huang, Y. Cai, H. Song, L. Wu, R. Cheng, Y. Li, S. Wang, H. Lyu, L. Zhang, J. Zhou, P. Liu, *Org. Lett.* **2018**, *20*, 5427–5430.
[29] E. Tamanaha, B. Zhang, Y. Guo, W. Chang, E. W. Barr, G. Xing, J. St Clair, S. Ye, F. Neese, J. M. Bollinger, C. Krebs, *J. Am. Chem. Soc.* **2016**, *138*, 8862–8874.
[30] E. P. Tchesnokov, A. S. Faponle, C. G. Davies, M. G. Quesne, R. Turner, M. Fellner, R. J. Souness, S. M. Wilbanks, S. P. de Visser, G. N. L. Jameson, *Chem. Commun.* **2016**, *52*, 8814–8817.
[31] P. R. Ortiz de Montellano, *Cytochrome P450*, Springer International Publishing, Cham, **2015**.
[32] J. M. Bollinger Jr, C. Krebs, *J. Inorg. Biochem.* **2006**, *100*, 586–605.
[33] L. Chen, N. Naowarojna, B. Chen, M. Xu, M. Quill, J. Wang, Z. Deng, C. Zhao, P. Liu, *ACS Catal.* **2019**, *9*, 253–258.
[34] L. M. K. Dassama, T. H. Yosca, D. A. Conner, M. H. Lee, B. Blanc, B. R. Streit, M. T. Green, J. L. DuBois, C. Krebs, J. M. Bollinger, *Biochemistry* **2012**, *51*, 1607–1616.
[35] A. R. McDonald, L. Que, *Coord. Chem. Rev.* **2013**, *257*, 414–428.
[36] M. M. Mbughuni, M. Chakrabarti, J. A. Hayden, E. L. Bominaar, M. P. Hendrich, E. Munck, J. D. Lipscomb, *Proc. Natl. Acad. Sci. USA* **2010**, *107*, 16788–16793.
[37] T. Harami, Y. Maeda, Y. Morita, A. Trautwein, U. Gonser, *J. Chem. Phys.* **1977**, *67*, 1164–1169.
[38] K. L. Stone, L. M. Hoffart, R. K. Behan, C. Krebs, M. T. Green, *J. Am. Chem. Soc.* **2006**, *128*, 6147–6153.
[39] C. E. Schulz, R. Rutter, J. T. Sage, P. G. Debrunner, L. P. Hager, *Biochemistry* **1984**, *23*, 4743–4754.
[40] X. Li, R. Fu, S. Lee, C. Krebs, V. L. Davidson, A. Liu, *Proc. Natl. Acad. Sci. USA* **2008**, *105*, 8597–8600.
[41] K. Rizzolo, S. E. Cohen, A. C. Weitz, M. M. López Muñoz, M. P. Hendrich, C. L. Drennan, S. J. Elliott, *Nat. Commun.* **2019**, *10*, 1101.
[42] A. C. Weitz, S. Biswas, K. Rizzolo, S. Elliott, E. L. Bominaar, M. P. Hendrich, *Inorg. Chem.* **2020**, *59*, 10223–10233.
[43] J.-U. Rohde, J.-H. In, M. H. Lim, W. W. Brennessel, M. R. Bukowski, A. Stubna, E. Münck, W. Nam, L. Que, *Science* **2003**, *299*, 1037–1039.
[44] M. R. Bukowski, K. D. Koehntop, A. Stubna, E. L. Bominaar, J. A. Halfen, E. Münck, W. Nam, L. Que, *Science* **2005**, *310*, 1000–1002.
[45] J. C. Price, E. W. Barr, B. Tirupati, J. M. Bollinger, C. Krebs, *Biochemistry* **2003**, *42*, 7497–7508.
[46] M. Newcomb, J. A. Halgrimson, J. H. Horner, E. C. Wasinger, L. X. Chen, S. G. Sligar, *Proc. Natl. Acad. Sci. USA* **2008**, *105*, 8179–8184.
[47] P. Chandrasekaran, S. C. E. Stieber, T. J. Collins, L. Que Jr., F. Neese, S. DeBeer, *Dalton Trans.* **2011**, *40*, 11070–11079.

[48] S. Sinnecker, N. Svensen, E. W. Barr, S. Ye, J. M. Bollinger, F. Neese, C. Krebs, *J. Am. Chem. Soc.* **2007**, *129*, 6168–6179.
[49] E. I. Solomon, S. D. Wong, L. V. Liu, A. Decker, M. S. Chow, *Curr. Opin. Chem. Biol.* **2009**, *13*, 99–113.
[50] D. Usharani, D. Janardanan, C. Li, S. Shaik, *Acc. Chem. Res.* **2013**, *46*, 471–482.
[51] M. Puri, L. Que, *Acc. Chem. Res.* **2015**, *48*, 2443–2452.

Manuscript received: July 2, 2023
Accepted manuscript online: August 28, 2023
Version of record online: ■■, ■■

Forschungsartikel

Non-Heme Iron Enzymes

J. C. Paris, S. Hu, A. Wen, A. C. Weitz, R. Cheng, L. B. Gee, Y. Tang, H. Kim, A. Vegas, W.-c. Chang,* S. J. Elliott,* P. Liu,* Y. Guo* **e202309362**

An $S=1$ Iron(IV) Intermediate Revealed in a Non-Heme Iron Enzyme-Catalyzed Oxidative C–S Bond Formation

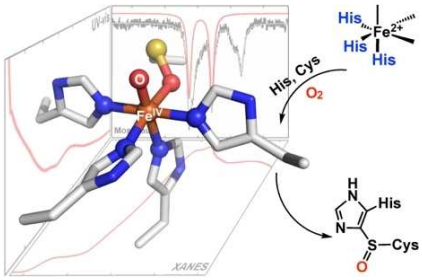

The first non-heme enzymatic $S=1$ Fe(IV) intermediate is discovered via transient kinetics and spectroscopic (Mössbauer, EPR, and XANES) characterizations. This novel species is a key intermediate to enable the oxidative carbon-sulfur bond formation in the biosynthesis of ovothiol A.